

1 This manuscript is an *EarthArXiv* preprint and it has been accepted for publication by
2 *Atmosphere*.

3

4 **Past and projected weather pattern persistence with** 5 **associated multi-hazards in the British Isles**

6 **Paolo De Luca^{1*}, Colin Harpham², Robert L. Wilby¹, John K. Hillier¹, Christian L. E. Franzke³ and**
7 **Gregor C. Leckebusch⁴**

8 ¹ Geography and Environment, Loughborough University, Loughborough, UK

9 ² Climatic Research Unit (CRU), School of Environmental Sciences, University of East Anglia, Norwich, UK

10 ³ Meteorological Institute and Center for Earth System Research and Sustainability (CEN), University of
11 Hamburg, Hamburg, Germany

12 ⁴ School of Geography Earth and Environmental Sciences, University of Birmingham, Birmingham, UK

13

14 * Correspondence: p.deluca@lboro.ac.uk

15 Received: date; Accepted: date; Published: date

16

17 **Abstract:** Hazards such as heatwaves, droughts and floods are often associated with persistent
18 weather patterns. Atmosphere-Ocean General Circulation Models (AOGCMs) are important tools for
19 evaluating projected changes in extreme weather. Here, we demonstrate that 2-day weather pattern
20 persistence, derived from the Lamb Weather Types (LWTs) objective scheme, is a useful concept for
21 both investigating climate risks from multi-hazard events as well as for assessing AOGCM realism.
22 This study evaluates the ability of a Coupled Model Intercomparison Project Phase 5 (CMIP5) multi-
23 model sub-ensemble of 10 AOGCMs at reproducing seasonal LWTs persistence and frequencies over
24 the British Isles. Changes in persistence are investigated under two Representative Concentration
25 Pathways (RCP8.5 and RCP4.5) up to 2100. The ensemble broadly replicates historical LWTs
26 persistence observed in reanalyses (1971-2000). Future persistence and frequency of summer
27 anticyclonic LWT are found to increase, implying heightened risk of drought and heatwaves. On the
28 other hand, the cyclonic LWT decreases in autumn suggesting reduced likelihood of flooding and
29 severe gales. During winter, AOGCMs point to increased risk of concurrent fluvial flooding-wind
30 hazards by 2100, however, they also tend to over-estimate such risks when compared to reanalyses.
31 In summer, the strength of the nocturnal Urban Heat Island (UHI) of London could intensify,
32 enhancing the likelihood of combined heatwave-poor air quality events. Further research is needed
33 to explore other multi-hazards in relation to changing weather pattern persistence and how best to
34 communicate such threats to vulnerable communities.

35 **Keywords:** weather patterns; LWTs; persistence; multi-hazards; urban heat island; CMIP5; RCPs

36

37 **1. Introduction**

38 Persistent weather patterns can translate into hazards such as heatwaves, poor air quality,
39 drought, wildfires and episodes of flooding [1–4], with significant socio-economic losses [5,6].

40 Examples of such impactful episodes include the 2003 and 2010 European summer heatwaves that
41 led to more than 100,000 deaths, reduced gross primary productivity of crops and, in the latter
42 episode over Russia, about US\$15 billion economic losses [7–10]. Similarly, summer 2013 in eastern
43 China, was the hottest ever recorded in that region, with persistent and widespread heatwaves and
44 droughts causing severe socio-economic impacts amounting to 59 billion RMB in losses [11].
45 Conversely, the extremely wet and stormy 2013/14 winter over the United Kingdom (UK) was
46 characterised by the passage of numerous low-pressure systems causing extensive pluvial, fluvial,
47 coastal and groundwater flooding along with severe gales [12–14].
48

49 Natural hazards pose a significant socio-economic threat, yet their spatio-temporal co-
50 occurrence (termed herein *multi-hazards*) are not yet fully understood [15,16]. Multi-hazards/risks
51 research has developed considerably over the last decade [17–21], such that the United Nations
52 Sendai Framework for Disaster Risk Reduction (UNDRR) [22] has called for multi-hazard approaches
53 to disaster risk reduction. Multi-hazards are also known as compound events [15,23]. Examples of
54 multi-hazard studies include interactions between earthquakes and landslides [24], multi-basin
55 fluvial flooding and extra-tropical cyclones [25], fluvial and coastal flooding [26–28], extreme wet and
56 dry hydrological events [29–31], and compound cold-wet dynamical extremes over different
57 continents [32]. Considering natural hazards as physical processes that can interact across both
58 temporal and spatial scales is of interest to decision makers such as government agencies, local
59 businesses, emergency management services and (re)-insurance companies. Natural hazards can
60 compound in various ways (i.e. occur simultaneously, as cascades or cumulatively) over a sufficiently
61 long time-frame [22], and therefore their combined socio-economic impacts can exceed what was
62 originally planned for, putting societies and economies under stress [15].
63

64 Daily atmospheric pressure patterns for the British Isles (BI) have been categorised according to
65 the system of Lamb Weather Types (LWTs) [33]. This classification was originally subjective, meaning
66 that daily weather patterns were assigned manually after inspection of weather charts. A few years
67 after the first subjective classification of LWTs [33], an objective method was developed to classify
68 daily atmospheric circulation according to LWTs [34]. Eventually, both the subjective and objective
69 approach were compared [35] and objective LWTs were subsequently derived from reanalysis
70 products [36]. The main novelty of the objective classification scheme is that it uses grid-point daily
71 mean sea-level-pressure (SLP) analysis for a fixed observation time (such as 00:00 or 12:00 UTC) [37].
72

73 Previous studies have investigated links between weather patterns (or large-scale atmospheric
74 circulation) and local extreme events, such as heavy rainfall, storms, floods and heatwaves [25,38–
75 46]. The conventional approach to fluvial flooding analysis at the *single* catchment scale is being
76 extended to frameworks with inter-related hazards, driven by global climate modes, covering
77 *multiple* catchments [39]. Others show that the bias in simulating regional extreme precipitation days
78 by an Atmosphere-Ocean General Circulation Model (AOGCM) is reduced by applying atmospheric
79 circulation indices [41]. Moreover, weather patterns extracted from AOGCMs have also been used to
80 downscale local climate variables, such as temperature, precipitation, radiation and humidity at local
81 scales [43,47,48]. However, AOGCMs vary in their ability to simulate the frequency, seasonality and
82 persistence of weather patterns at regional scales [42,43].

83

84 Some studies have linked heavy precipitation events to atmospheric circulation states, such as
85 the 850hPa geopotential height field or integrated vapour transport (IVT) [40], and found connections
86 between LWTs [33–35], and multi-basin fluvial flooding driven by extra-tropical cyclones (ETCs) [25].
87 In the latter scenario, major widespread floods in Great Britain (GB), observed during December 1979,
88 October 2000, December 2002–January 2003, November–December 1992 and January–February 1995,
89 were mostly driven by cyclonic and westerly LWTs [25]. Others have used LWTs to reconstruct the
90 synoptic drivers of fluvial floods in GB since the 1870s [49]. Furthermore, some work uses LWTs to
91 quantify changes in the strength of the *nocturnal Urban Heat Island (UHI)* – a phenomenon that may
92 be associated with combined heatwave and air pollution events within cities [38,50], and is mainly
93 driven by anticyclonic weather patterns.. The LWTs classification scheme, although initially
94 developed for the UK [25,36,58–63,45,51–57], was also recently applied in other mid-latitude regions,
95 for example Sweden [64,65], the Iberian Peninsula [66,67] and Spain [68,69]. As far the authors are
96 aware, no study has yet investigated links between LWTs and multi-hazards in AOGCMs projections
97 up to 2100. Such an assessment could raise awareness of risks thereby informing resilience and
98 disaster risk reduction measures, from local to regional scales.

99

100 Previous evaluations for Europe and the BI show that Coupled Model Intercomparison Project
101 Phase 5 (CMIP5) AOGCMs generally reproduce LWTs, calculated using daily sea-level pressure
102 (SLP) fields, but there are recognized biases [53,54]. For example, CMIP5 AOGCMs are not yet able
103 to simulate correctly the number of anticyclonic (A-type) patterns and hence blocking episodes, with
104 the former being underestimated in northern Europe and the BI, but overestimated in southern
105 Europe [53,54,70]. Other biases are found for cyclonic (C-type) and westerly (W-type) occurrences,
106 with both being overestimated across Europe [54]. These studies also examined future changes in
107 frequency of LWTs and blocking episodes by comparing historical conditions with RCP8.5, to
108 determine how such changes might affect European temperatures. The A-type is projected to increase
109 significantly over the BI during all seasons except for winter (DJF), the C-type to decrease in all
110 seasons, and the W-type to increase except in summer (JJA) by the end of the century [54]. Overall,
111 blocking episodes are projected to decrease for the BI in DJF and JJA by 2061–2090 (RCP8.5) [70].

112

113 We extend these analyses by assessing the ability of a CMIP5 [71] multi-model sub-ensemble
114 (MME) of 10 AOGCMs at reproducing historical seasonal persistence of daily LWTs over the BI [33–
115 36]. We define 2-day persistence as the probability that a given LWT will occur on any two successive
116 days. Climate model simulations of historic LWTs are compared with those derived from 20CR [72],
117 NCEP [73] reanalyses, and Lamb’s catalogue of subjectively defined weather types [33,74]. We
118 investigate how persistence and seasonal frequencies are projected to change within the full 21st
119 century under RCP8.5 and RCP4.5, with persistence assessed for both the MME mean (MMEM) and
120 individual AOGCMs. We also quantify and discuss the implications of future multi-hazards, here
121 identified as nearly concurrent multi-basin fluvial flooding and ETCs impacting GB in winter [25] or
122 combined summer heatwave and poor air quality events over London [38]. Thus, two multi-hazard
123 metrics are applied, along with their evaluation under RCP8.5 and RCP4.5 projections up to 2100.

124 These are the likelihood of (1) multi-basin fluvial flooding linked with ETCs (*F-Score*) and (2)
 125 changing intensity of the nocturnal UHI.

126

127

128 2. Methods and Data

129 2.1 Lamb Weather Types (LWTs)

130 Daily atmospheric sea-level pressure (SLP) patterns are categorized using the system of LWTs
 131 [33] via an objective classification scheme centred over the BI (Figure 1) [34,35]. Choice of the LWTs
 132 objective scheme is justified by the fact that this methodology and weather typing classification was
 133 originally developed for the BI. LWTs of similar airflow properties are derived from a 5° by 10°
 134 latitude-longitude grid array (Figure 1) and computed from daily (12 UTC) SLP values at each grid
 135 point. The airflow characteristics are expressed by the following set of equations, where the integers
 136 in bold correspond to the grid point reference numbers in Figure 1:

137

$$138 \quad W = \frac{1}{2}(SLP_{12} + SLP_{13}) - \frac{1}{2}(SLP_4 + SLP_5) \quad (\text{westerly flow}) \quad (\text{Eq. 1})$$

139

$$140 \quad S = 1.74 \left[\frac{1}{4}(SLP_5 + 2.0 \times SLP_9 + SLP_{13}) - \frac{1}{4}(SLP_4 + 2.0 \times SLP_8 + SLP_{12}) \right]$$

$$141 \quad (\text{southerly flow}) \quad (\text{Eq. 2})$$

142

$$143 \quad F = (S^2 + W^2)^{1/2} \quad (\text{resultant flow}) \quad (\text{Eq. 3})$$

144

$$145 \quad ZW = 1.07 \left[\frac{1}{2}(SLP_{15} + SLP_{16}) - \frac{1}{2}(SLP_8 + SLP_9) \right] - 0.95 \left[\frac{1}{2}(SLP_8 + SLP_9) - \frac{1}{2}(SLP_1 + SLP_2) \right]$$

$$146 \quad (\text{westerly shear vorticity}) \quad (\text{Eq. 4})$$

147

$$148 \quad ZS =$$

$$149 \quad 1.52 \left[\frac{1}{4}(SLP_6 + 2.0 \times SLP_{10} + SLP_{14}) - \frac{1}{4}(SLP_5 + 2.0 \times SLP_9 + SLP_{13}) - \frac{1}{4}(SLP_4 + 2.0 \times SLP_8 + SLP_{12}) \right] \\ + \frac{1}{4}(SLP_3 + 2.0 \times SLP_7 + SLP_{11})$$

$$150 \quad (\text{southerly shear vorticity}) \quad (\text{Eq. 5})$$

151

$$152 \quad Z = ZW + ZS \quad (\text{total shear vorticity}) \quad (\text{Eq. 6})$$

153

154 Flow units are derived from the geostrophic approximation (each equivalent to 1.2 knots) and
 155 they are, along with the geostrophic vorticity units, expressed as hPa per 10° latitude at 55°N (100
 156 units are equivalent to $0.55 \times 10^{-4} = 0.46$ times the Coriolis parameter at 55°N). Three coefficients are
 157 used within Eqs. 2, 4 and 5 to account for variations in relative grid spacing at different latitudes with
 158 latitude (ψ) here set as 55° [34]: *S* is multiplied by 1.74, derived from $1/\cos(\psi)$; *ZW*, 1.07 and 0.95 from
 159 $\sin(\psi)/\sin(\psi-5^\circ)$ and $\sin(\psi)/\sin(\psi+5^\circ)$; *ZS*, 1.52 from $1/2(\cos(\psi)^2)$.

160

161 The last step for defining LWTs is to apply five rules [33–35]:

162
163
164
165
166
167
168
169
170
171
172
173
174
175
176
177
178
179

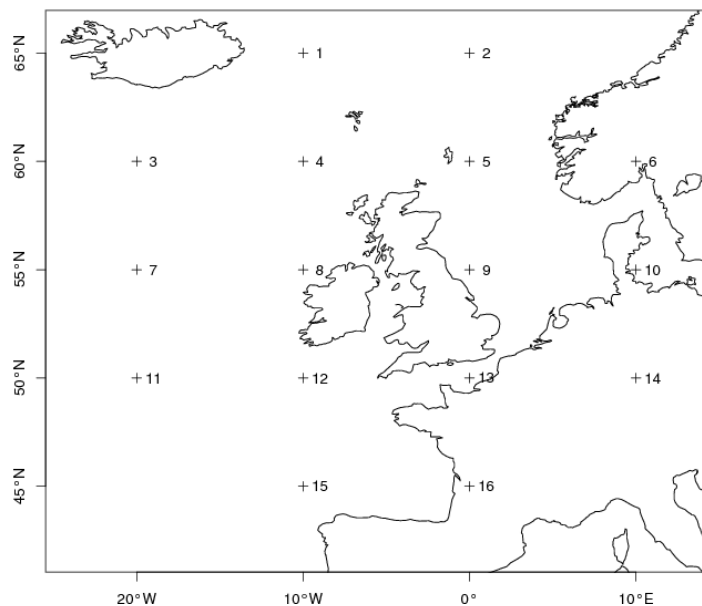
1. Flow direction is given by $\tan^{-1}(W/S)$ and is calculated on an eight-point compass with 45° per sector. If W is positive, add 180° . Thus, the W -type occurs between 247.5° and 292.5° (Eqs. 1-2);

2. Lamb pure directional weather types (e.g. N, S, or E-types) correspond to an essentially straight flow, when $|Z|$ is less than F (Eq. 6);

3. Lamb's pure cyclonic (C) and anticyclonic (A) types are identified when $|Z|$ is greater than $2F$, respectively with $Z > 0$ and $Z < 0$ (Eqs. 3 and 6);

4. Lamb's hybrid types (e.g. AE and CSW) are characterised by a flow partially anticyclonic/cyclonic, with $|Z|$ lying between F and $2F$ (Eqs. 3 and 6);

5. An unclassified (U) type is obtained when F and $|Z|$ are less than 6, with the choice of 6 depending on grid spacing, meaning that if using a grid resolution finer than 5° by 10° latitude-longitude it needs to be tuned (Eqs. 3 and 6).



180
181
182
183
184

Figure 1. Grid points used to calculate Jenkinson flow and vorticity terms for the British Isles (BI). Numbers refer to those points used in Equations 1 to 5.

185 The objective classification scheme yields 27 LWTs comprised of two synoptic types
186 (anticyclonic A and cyclonic C), five purely directional types (westerly W, north-westerly NW,
187 easterly E, northerly N, and southerly S), 19 hybrid combinations of synoptic and directional types
188 (e.g. CNW, CSE and AE), and 1 unclassified (U) type (Table 1) [33–35,75]. For persistence and
189 frequency analyses, we focus on the 7 synoptic and directional LWTs plus the U-type; counts of
190 hybrid types were spread across the main types as per Lamb's original definition [33,76] and common

191 practice within earlier studies [35–37,77]. We assess LWT persistence and frequency for summer
 192 (June-July-August, JJA), autumn (September-October-November, SON), winter (December-January-
 193 February, DJF) and spring (March-April-May, MAM). When calculating indices of future multi-
 194 hazards, hybrid LWTs were not incorporated into the 7 main types as the F-Score and nocturnal UHI
 195 indices require these individual weather patterns to be considered independently. For a more
 196 detailed description with maps showing the pressure patterns associated with the main LWTs we
 197 refer the reader to [33,34].

198
 199

200 **Table 1. Description of the seven main LWTs and unclassified (U) type [33,75].**

LWT	Description
Anticyclonic (A)	Anticyclones centred over, near, or extending over the British Isles.
Cyclonic (C)	Depressions passing frequently or stagnating over the British Isles. The central isobar of the depression should extend over the mainland of Britain or Ireland.
Westerly (W)	High pressure to the south and low pressure to the north, giving a sequence of depressions travelling eastward across the Atlantic. This is the main, progressive zonal type.
North-westerly (NW)	Azores anticyclone displaced northeast or north towards the British Isles. Depressions forming near Iceland and travelling south-east into the North Sea.
Easterly (E)	Anticyclones over Scandinavia extending towards Iceland across the Norwegian Sea. Depressions generally to the south of the region over south-west Europe and the western Atlantic.
Northerly (N)	High pressure to the west or northwest of Britain extending from Greenland southwards, possibly as far as the Azores. Depressions travel southward from the Norwegian Sea.
Southerly (S)	High pressure over central and northern Europe. Depressions blocked to the west or travelling north or north-eastwards off western coasts.
Unclassified (U)	Weather pattern weak or chaotic.

201
 202

203 2.2 Data

204 Weather patterns were derived from the SLP produced by each AOGCM in our CMIP5 MME
 205 listed in Table 2 [71]. CMIP5 data were obtained from the World Climate Research Programme
 206 (WCRP, <https://esgf-node.llnl.gov/projects/cmip5/>). We defined the historical period as the 1980s
 207 (1971-2000) whereas the future was divided into three 30-year periods: the 2020s (2011-2040), 2050s
 208 (2041-2070) and 2080s (2071-2100). Such subdivision of time-periods is common practice within the
 209 climate modelling community [e.g. 20,78,79], as it allows us to evaluate information belonging to four
 210 30-year periods up to 2100. We note that CMIP5 observational runs are available from 1950-2005 and
 211 future RCP runs cover the period 2006-2100. The CMIP5 AOGCMs and MMEM outputs for the
 212 historical period were compared with LWTs derived from 20CR [72], NCEP [73] reanalyses and
 213 Lamb’s subjective catalogue, which ends in 1997 and was based on observed daily surface and mid-
 214 troposphere (500 mb) pressure charts at noon [33,74]. The 20CR reanalysis product is derived by
 215 making use of synoptic surface pressure observations. This has a spatial resolution of 2°×2° (latitude
 216 × longitude) and covers the 1871-present period with 6h time steps and 28 pressure levels [72]. On
 217 the other hand, NCEP reanalysis is computed from a different set of observations (e.g. land surface,

218 ship, aircraft and satellite), and covers the period 1948-present with 2.5°×2.5° (latitude × longitude)
 219 spatial resolution, 6h time steps and 17 pressure levels [73]. Both 20CR and NCEP datasets are largely
 220 used for climate model evaluations and their biases can be summarised as follows: i) 20CR
 221 overestimates cloud fraction and precipitation [80]; and ii) NCEP underestimates the temperature,
 222 overestimates the wind-speed and monthly precipitation variability [81]. The MMEM was built by
 223 first deriving the LWTs and their seasonal persistence and frequencies in each AOGCM, then
 224 averaging these metrics within each time-period. The choice of the models included in our MME
 225 (Table 2) reflects a range of research institutes running similar boundary forcing experiments.

226
 227
 228

Table 2. CMIP5 multi-model sub-ensemble (MME) used in the analyses.

Model name	Research institute	Lat-Lon resolution	Ensemble member
HadGEM2-ES	Met Office, United Kingdom	1.25° × 1.875°	r1i1p1
MPI-ESM-LR	Max Planck Institute for Meteorology, Germany	1.9° × 1.9°	r1i1p1
MRI-CGCM3	Meteorological Research Institute, Japan	1.1° × 1.1°	r1i1p1
CNRM-CM5	National Centre for Meteorological Research, France	1.4° × 1.4°	r1i1p1
CanESM2	Canadian Center for Climate Modeling and Analysis, Canada	2.8° × 2.8°	r1i1p1
MIROC5	Model for Interdisciplinary Research on Climate, Japan	1.4° × 1.4°	r1i1p1
CSIRO-Mk3.6.0	Commonwealth Scientific and Industrial Research Organisation, Australia	1.9° × 1.9°	r10i1p1
IPSL-CM5A-LR	Institute Pierre-Simon Laplace, France	1.9° × 3.75°	r1i1p1
CCSM4	National Center for Atmospheric Research, USA	0.94° × 1.25°	r6i1p1
GFDL-CM3	Geophysical Fluid Dynamics Laboratory, USA	2° × 2.5°	r1i1p1

229 The columns in Table 2 show the: (1) CMIP5 model name; (2) research institute where the model was
 230 developed; (3) resolution for latitude by longitude in degrees; and (4) ensemble member analysed.
 231 For all models the historical and RCP8.5 (and RCP4.5) sea-level pressure (SLP) outputs are used to
 232 calculate daily LWTs for the BI.

233
 234

235 2.3 Persistence and trend analyses

236 Weather pattern persistence is defined here as the conditional probability (p_{ji}) that a given LWT_j
 237 on day(t) is followed by the same LWT_j on day($t+1$) [82,83]. This diagnostic was extracted for the 7
 238 main LWTs and the U-type using the diagonal cells of Markov-chain transition matrices. This enabled

239 estimation of historical (1980s) and future (2020s, 2050s and 2080s) seasonal persistence for the
 240 MMEM as well as for individual AOGCMs for impactful weather types and seasons, the 20CR, NCEP
 241 reanalyses and Lamb’s subjective catalogue.

242

243 Uncertainty in p_{jj} for the 1980s was calculated by boot-strapping ($n=1,000$) 30-year seasonal
 244 simulations using the *markovchain* package within the R framework [84]. This algorithm stochastically
 245 generates n series of daily LWTs from the original conditional distributions of the weather patterns
 246 in each AOGCM, then recomputes p_{jj} from each series. The resulting $p^{BOOTSTRAP_{jj}}$ is the mean of all p_{jj}
 247 across the 1000 series, for each AOGCM. The 95% confidence intervals of $p^{BOOTSTRAP_{jj}}$ are obtained from
 248 the cumulative distribution of the 1000 values of p_{jj} for each AOGCM.

249

250 Statistical significance of changes in persistence for the AOGCM sub-ensemble between the
 251 1980s and future periods (Tables S1-S2) was assessed using a Mann-Whitney-Wilcoxon two-tailed
 252 test [85] applied to the 10 estimates of $p^{BOOTSTRAP_{jj}}$ for each time period. Changes in p_{jj} between the
 253 1980s and future periods for *individual* AOGCMs were regarded as statistically significant if future
 254 persistence of a given LWT and AOGCM fell outside the 95% confidence intervals of the $p^{BOOTSTRAP_{jj}}$
 255 range of that AOGCM for the 1980s.

256

257 To detect both linear and non-linear annual changes in the total seasonal counts of LWTs MMEM
 258 frequencies under RCP8.5 and RCP4.5 scenarios, a trend analysis was performed for the entire 2006-
 259 2100 time-period. For illustrative purposes, we only show trends for anticyclonic (A, summer JJA),
 260 cyclonic (C, autumn SON) and westerly (W, winter DJF) types as indicators of impactful weather
 261 across the BI. Results are also presented for the southerly (S, spring MAM) types as this LWT shows
 262 most significant changes in seasonal persistence according to the non-parametric Mann-Whitney-
 263 Wilcoxon two-tailed test between the 1980s and each of the three future periods (i.e. 2020s, 2050s and
 264 2080s). A modified Mann-Kendall test, which takes into account possible autocorrelation within the
 265 time series, was applied to both RCP8.5 and RCP4.5 seasonal MMEM LWTs frequencies [86]. The
 266 significance of trends, along with their relative Sen’s slopes, are shown in Table S3 [87].

267

268 2.4 Indices of winter fluvial flooding-wind hazards and summer UHI intensity

269

270 As a measure of concurrent fluvial flooding-wind hazards we calculated an extended version of
 271 the F-Index [25,49], here defined as the F-Score, for each AOGCM, MMEM, 20CR, NCEP and Lamb’s
 272 subjective catalogue, covering the 1980s, 2020s, 2050s and 2080s, for selected LWTs known to drive
 273 these multi-hazard events [25] during winter under both RCP8.5 and RCP4.5. The F-Index is the ratio
 274 of observed to expected frequency of fluvial floods for a given LWT, where values greater than 1
 275 show higher than expected likelihood. Ten LWTs are known to be associated with historic, multi-
 276 basin fluvial floods [25], of which eight (C, CS, CSW, CNW, S, SW, W, and NW-types) increase their
 277 likelihood and two (N and A-types) reduce likelihood. All other LWTs are weighted zero. The F-
 278 Score, for each AOGCM, is then calculated by multiplying the winter DJF frequencies ($freq_djf_j$) of
 279 these LWTs by their F_Index_j (as per Event Set E in [25]) and by summing these values:

279

$$280 \quad F_Score_i = \sum_{j=1}^{10} freq_djf_{i,j} \times F_Index_{i,j} \quad (Eq. 7)$$

281

282 where i represents the single AOGCM, 20CR, NCEP and Lamb's subjective datasets within the
283 relative time periods of 1980s, 2020s, 2050s, 2080s and j is the given LWT considered from the 10
284 types mentioned above. The higher the F-Score, the greater the likelihood of concurrent multi-basin
285 fluvial flooding and wind hazards within winter, over the specified time horizon and RCP scenario.

286

287 As a proxy for combined heatwave and poor air quality hazards occurring during summer, we
288 use observed, simulated and projected nocturnal UHI temperatures in tenths of degree Celsius for
289 London (UK) [38], using the same datasets, time periods and RCPs as per the F-Score. The UHI
290 phenomenon is caused by absorption and trapping of heat as well as by changed airflows and
291 sensible heat fluxes within the built environment. The simplest form of UHI metric (used by [38]) is
292 based on the daily temperature difference between an urban and rural reference site (during daylight
293 or night hours). These values may then be stratified by LWT to show the extent to which some
294 weather patterns favour extreme UHI episodes. Previous studies show that the anticyclonic (A)
295 weather types are associated with extreme UHI events [38,50]. The UHI metric, for each AOGCM,
296 was derived as follows by: i) multiplying LWT summer JJA frequencies ($freq_jja_h$) by their
297 respective average UHI intensities taken from [38] (UHI_w_h); ii) summing these values; and iii)
298 dividing the total from step ii) by the number of days in the period analysed ($days_h$) to give the mean
299 daily UHI intensity:

300

$$301 \quad UHI_i = \sum_{h=1}^{27} \frac{freq_jja_{i,h} \times UHI_w_{i,h}}{days_{i,h}} \quad (Eq. 8)$$

302

303 where i is the same notation as per the F-Score and h refers to the 27 LWTs.

304

305 To assess the statistical significance of changes in the AOGCM output for the 1980s and future
306 2020s, 2050s and 2080s periods (for both the F-Score and nocturnal UHI temperatures) we applied a
307 similar approach as per persistence. Here, $n=1,000$ boot-strapped samples of daily LWT series (based
308 on conditional distributions for all seasons combined) were generated for each AOGCM run in the
309 1980s. Next, the F-Score or UHI were calculated for every series and AOGCM, then averaged and
310 confidence limits established as before. This procedure shows the extent to which estimates for the
311 future indices fall within the 95% confidence range of the boot-strapped estimate for each AOGCM
312 in the 1980s.

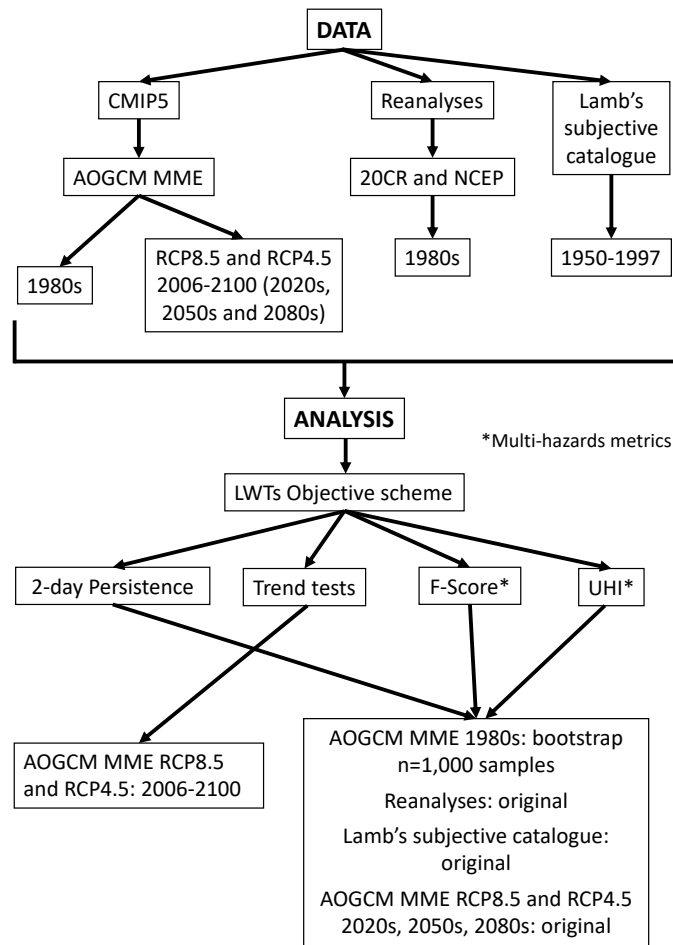
313

314 Sample sizes varied depending on the index and AOGCM. For the F-Score, we considered the
315 period 1971-2001 to capture January and February of winter 2000/01. Here, models with leap years
316 have a total of 11,323 days, models without leap years 11,315 days and the HadGEM2-ES model (with
317 360 days per year) has 11,160 days. For the UHI, the calendar years 1971-2000 were used as we are
318 interested in summer temperatures, with leap year AOGCMs having 10,958 days, non-leap years
319 models 10,950 days and the HadGEM2-ES 10,800 days.

320

321 Figure 2 provides a synthesis of the data and methodological framework.

322
323



324
325
326
327
328

Figure 2. Main data and methodology steps. The figure synthesise the procedures described in Section 2. Methods and Data.

3 Results

3.1 Persistence of weather patterns (MME)

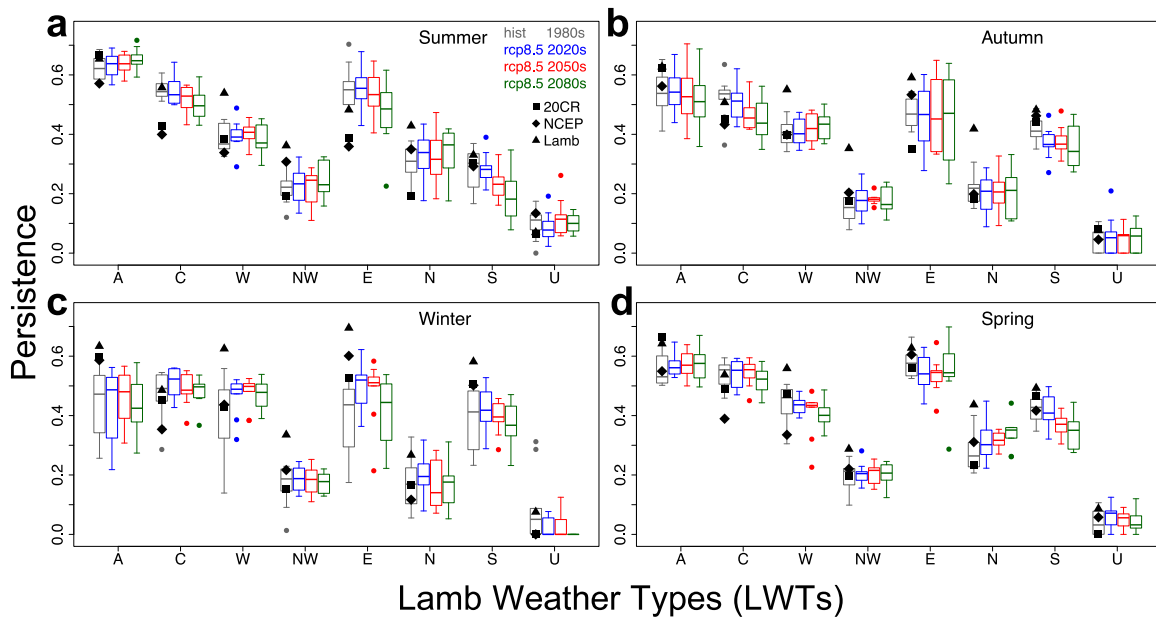
The A, C and W patterns are the most frequent weather types affecting the BI. Overall, the MME replicates weather type persistence during the four climatological seasons when compared with 20CR [72] and NCEP [73] reanalyses for the historical period (1980s) (Figure 3). There is less agreement between Lamb's subjectively classified daily weather catalogue and both the MME and reanalyses. A-type persistence is more variable within the MME and on average underestimated in winter, consistent with previous studies [53,54]. There is closer agreement for the A-type in other seasons.

337
338
339
340
341
342

W-type persistence agrees with the reanalyses but is always less than in Lamb's catalogue. C-type persistence is overestimated by the MME in all seasons when compared to reanalyses as reported before [54] for Europe more generally. Such biases in the C-type could be interpreted as exaggerating the likelihood of flooding in the MME compared with reanalyses [49].

343 Figure 3 shows that the distributions of persistence are asymmetrical (or skewed) around the
 344 MME means for many of the weather types and time periods. This characteristic suggests potentially
 345 large biases in the estimation of extreme events, if relying on a single AOGCM. Changes in weather
 346 type persistence between the ensembles of historical and future periods within RCP8.5 (Figure 3) are
 347 weakly significant (p -value <0.1 , Mann-Whitney-Wilcoxon two-tailed test) for the C-type in summer
 348 and autumn by 2080s; W-type in winter by 2050s; E-type in summer by 2080s and winter for the 2020s
 349 and 2050s; N-type in spring by 2050s and 2080s; and S-type in summer by 2080s, autumn in all periods
 350 and spring by 2050s and 2080s (Table S1).

351
 352



353
 354 **Figure 3. Persistence of the seven main LWTs plus unclassified (U) type under RCP8.5.** Persistence
 355 is calculated for (a) summer, (b) autumn, (c) winter and (d) spring, for the historical 1980s (1971-2000)
 356 and under RCP8.5 by the 2020s (2011-2040), 2050s (2041-2070) and 2080s (2071-2100). Boxplots show
 357 distributions of persistence in each LWT, for the 10-member AOGCM ensemble, compared with
 358 20CR, NCEP and the Lamb's catalogue. Segments show the minimum, 1st quartile, median, 3rd
 359 quartile and maximum. Outliers are shown by dots.

360
 361

362 Results for RCP4.5 show similar changes in persistence compared to RCP8.5, although they are
 363 smaller (Figure S1). In particular, the C-type is found to change significantly ($p<0.1$) only in summer
 364 by the 2080s; the E-type in winter by the 2080s; the N-type only in spring by the 2080s; and the S-type
 365 in summer by the 2050s and spring also by the 2020s (Table S2).

366
 367

3.2 Persistence of weather patterns (by model)

368 Figure 4 shows persistence for the same future periods but for each AOGCM in the MME
 369 compared with the reanalyses and Lamb's catalogue, for impactful weather types and seasons.
 370 Significance of changes was assessed against the boot-strapped confidence limits for the 1980s. Most
 371 model projections under RCP8.5 fall outside the 95% confidence intervals of historical persistence. A-

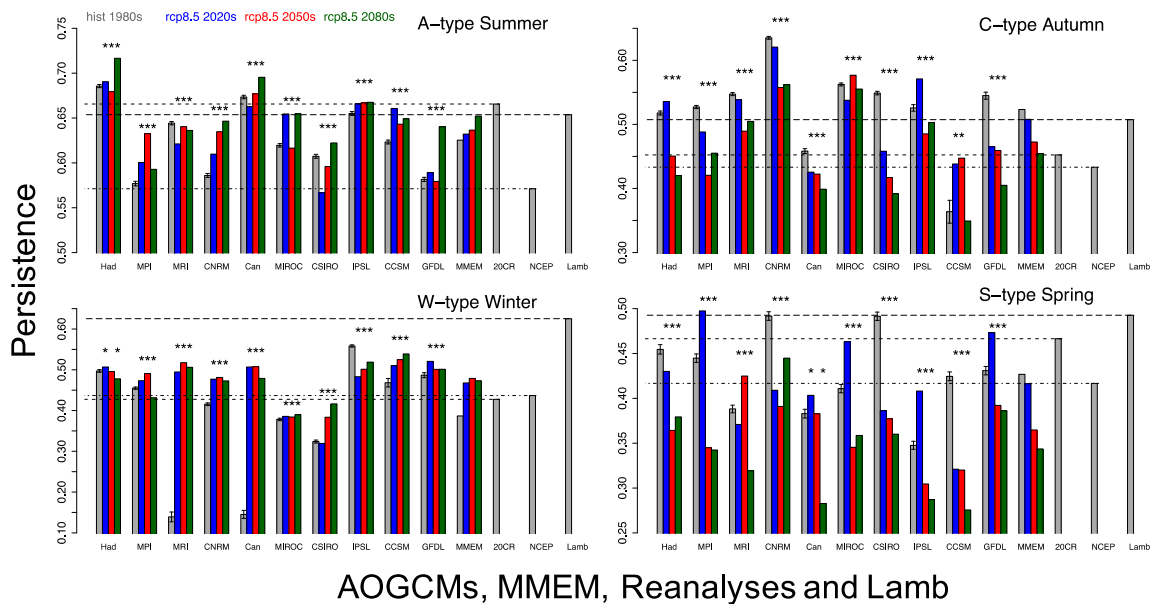
372 type MMEM persistence increases during summer (Figures 3a and 4a); C-type persistence decreases
 373 in all seasons, most markedly in summer and autumn (Figures 3 and 4b); W-type persistence does
 374 not change in winter but increases in autumn and decreases in spring (Figures 3b-d and 4c).

375

376 Amongst the other weather types, we note only a decrease in C- and E-types during summer, an
 377 increase in N-type in spring, and S-type persistence decreases in all seasons (Figures 3 and 4d). The
 378 AOGCMs showing the largest change in A-type persistence during summer are CNRM-CM5, GFDL-
 379 CM3 and MIROC5, with a significant increase of 0.06, 0.06 and 0.04 respectively between 1980s and
 380 2080s. For the C-type in autumn, CSIRO-Mk3.6.0, GFDL-CM3 and HadGEM2-ES show a significant
 381 decrease in persistence, between 1980s and 2080s, of 0.16, 0.14 and 0.10 respectively. During winter,
 382 for the W-type, the AOGCMs showing the largest change, between the same 1980s and 2080s periods,
 383 are MRI-CGCM3, CanESM2 and CSIRO-Mk3.6.0 with a significant increase in persistence of 0.37, 0.33
 384 and 0.09 respectively.

385

386



387

388 **Figure 4. Persistence of selected LWTs and seasons for individual AOGCMs under RCP8.5.** (a)
 389 A-type (summer), (b) C-type (autumn), (c) W-type (winter) and (d) S-type (spring) in the 1980s
 390 compared with the 2020s, 2050s and 2080s under RCP8.5. Persistence is shown for individual
 391 AOGCMs alongside the MMEM, 20CR, NCEP and Lamb's catalogue. Asterisks (*) show model runs
 392 with persistence outside the 95% confidence intervals of the boot-strapped (n=1,000) estimates for the
 393 1980s, shown here as black T-bars. Dashed lines represent the reanalyses and Lamb's catalogue
 394 values.

395

396

397 Analysis of RCP4.5 output shows similar, though less marked, results when compared to RCP8.5
 398 (Figure S2). Under the lower emission scenario, we find that most AOGCMs project persistence that
 399 falls outside the 95% confidence intervals of the 1980s. A-type MMEM persistence in summer could
 400 increase slightly, in particular during the 2080s (Figures S1a-S2a), C-type in autumn may decrease

401 (Figures S1b-S2b), W-type during winter is projected to remain stable across the three future periods
 402 (Figures S1c-S2c) and S-type persistence in spring decreases by 2100 (Figures S1d-S2d). The C-type
 403 in summer and A-type in autumn exhibit decreased persistence, whereas the E-type shows a marked
 404 increase in persistence during winter; findings that differ from RCP8.5 (Figure S1).

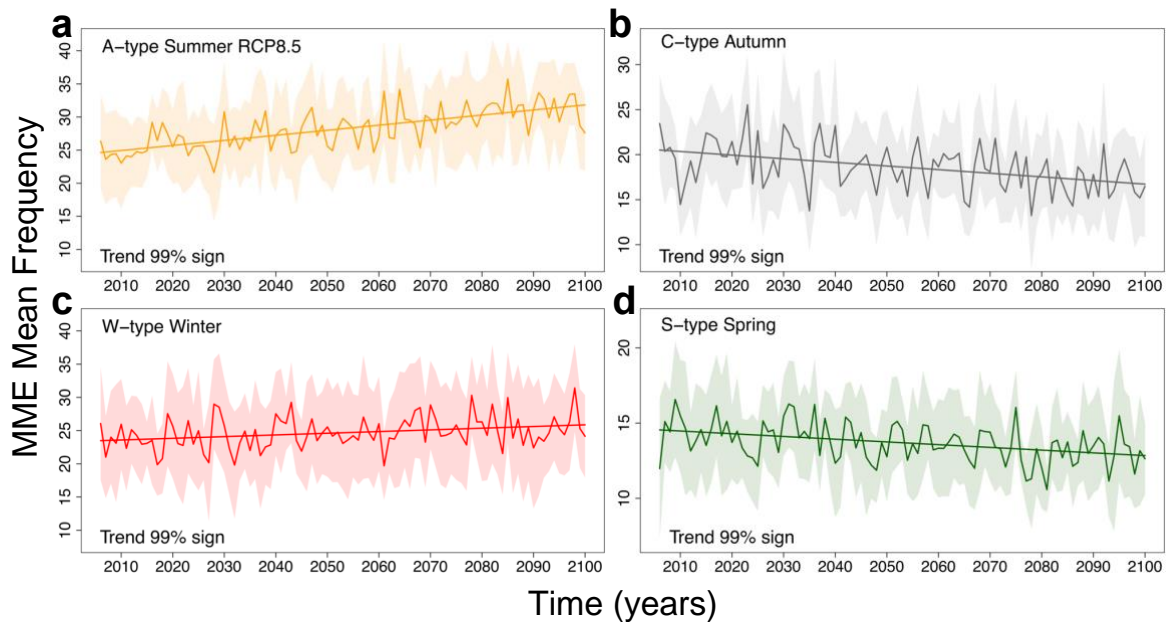
405

406 *3.3 Frequency of weather patterns (MMEM)*

407 Projected frequency trends for selected weather types and seasons under RCP8.5 (2006-2100) are
 408 shown in Figure 5. Summer A- and winter W-type frequencies could rise significantly ($p < 0.01$, Table
 409 S3) by 0.8 and 0.2 days per decade respectively over the period 2006-2100. Conversely, C- and S-type
 410 frequencies decrease significantly ($p < 0.01$, Table S3) in autumn and spring respectively. No
 411 significant trends are found for C-type frequency during winter. Sen's slopes for the MMEM with
 412 their statistical significance are given in Table S3 for each weather type, season and RCP. We also
 413 computed the Sen's slopes for A-type in each AOGCM during summer (RCP8.5, not shown here) to
 414 check whether the increase in A-type was solely due to a few models showing a large increase in this
 415 weather type. We found that all models within the MME show a positive increase in A-type
 416 frequency, with 7 out of 10 AOGCMs showing significance at the 90% level, with no outliers skewing
 417 the MMEM. Among other seasons (not shown), a significant decrease in annual frequencies is
 418 observed for the C-type during summer ($p < 0.01$) and spring ($p < 0.05$), along with a significant ($p < 0.01$)
 419 increase in A-type during spring, which all reflect the changes in persistence (Figure 3a and 3d).

420

421



422

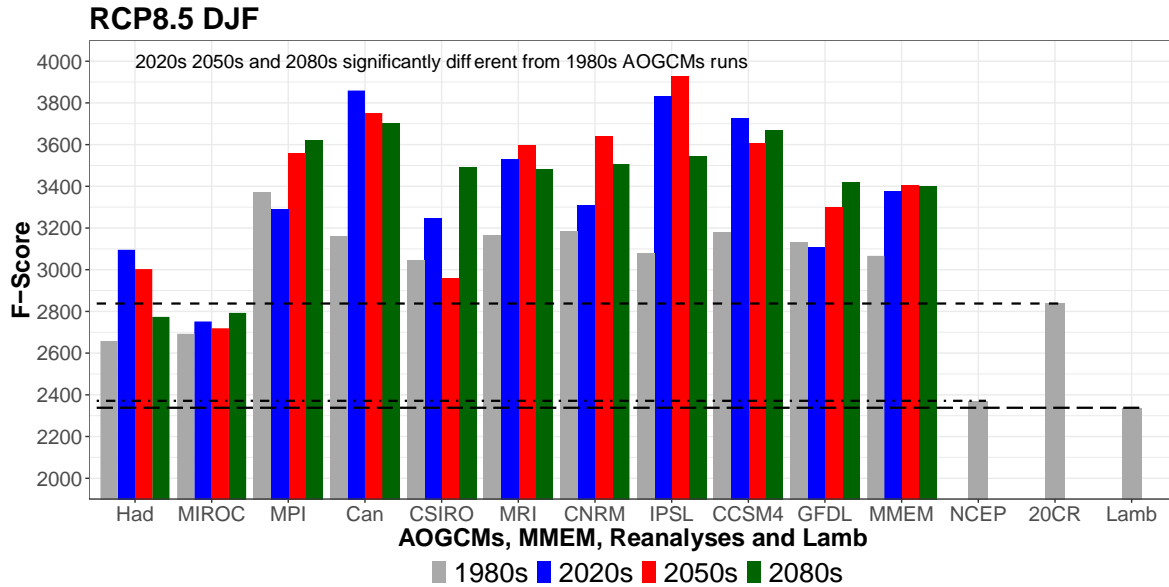
423 **Figure 5. Projected annual frequencies for selected LWTs and seasons under RCP8.5.** Frequencies
 424 are shown as MMEM for (a) summer anticyclonic A, (b) autumn cyclonic C, (c) winter westerly W
 425 and (d) spring southerly S LWTs under RCP8.5 (2006-2100). Trends are statistically significant at the
 426 1% level ($p\text{-value} < 0.01$, modified Mann-Kendall test). Shaded areas represent the 95% confidence
 427 intervals of the MMEM. The trend lines refer to the Sen's slopes calculated with the modified Mann-
 428 Kendall test.

429
430
431
432
433
434
435
436
437
438
439
440
441
442
443
444
445
446
447
448
449
450
451
452
453
454
455
456
457
458
459
460
461

Projections of MEM frequencies for the same LWTs and seasons but under RCP4.5 are shown in Figure S3 and Table S3. Results for RCP4.5 reflect the scenarios of RCP8.5 although the Sen's slopes are less extreme and statistically significant. The A-type frequency is projected to increase significantly ($p < 0.01$, Figure S3a and Table S3) during summer, C-type in autumn is set to decrease ($p < 0.05$, Figure S3b), W-type frequency in winter shows no significant trend (Figure S3c), and the S-type during spring decreases significantly ($p < 0.05$, Figure S3d). As per RCP8.5, we also observe (not shown) a significant decrease in C-type frequencies during summer ($p < 0.01$) and spring ($p < 0.05$) and an increase in the A-type during spring ($p < 0.05$), matching the relative changes in persistence (Figure S1a and S1d).

3.4 Application to future multi-hazards

In Figure 6 we extend an earlier analysis [25] based on impactful LWTs found to generate concurrent fluvial flooding-wind hazards in GB (see Section 2.4). Thus, the F-Score for each single AOGCM, MEM, 20CR, NCEP and Lamb's subjective datasets and 1980s, 2020s, 2050s and 2080s time periods are shown for winter DJF weather patterns under RCP8.5. The F-Score is a measure of the severity of future concurrent fluvial flooding-wind hazards, such that higher values represent more severe impacts compared to lower ones. Here, we show that the baseline risk from multiple flood-wind hazards is overestimated by all but two of the AOGCMs (HadGEM2-ES and MIROC5) when compared to NCEP, 20CR reanalyses and Lamb's subjective catalogue for the 1980s. Assuming the same bias holds in the future, the AOGCMs evaluated here likely overestimate *absolute* future risk from concurrent flood-wind hazards by 2100. Moreover, in a similar way as per Figure 4, there exists a large variability between the AOGCMs, so F-Score results are mixed with some AOGCMs suggesting increased/decreased risk of flood-wind hazards by the end of the 21st century. Lastly, by looking at the MEM we conclude that, although overestimated by AOGCMs, future risk from concurrent flood-wind hazards could increase by 2100 compared with the 1980s. Among the AOGCMs, those showing the largest F-Score increase between the 1980s and 2080s are CanESM2, CCSM4 and IPSL-CM5A-LR. Results for RCP4.5 are shown in Figure S4 and they agree with what was found for RCP8.5, with large variability amongst AOGCMs and MEM F-Score even slightly higher than RCP8.5.



462

463

464

465

466

467

468

469

470

471

472

473

474

475

476

477

478

479

480

481

482

483

484

485

486

487

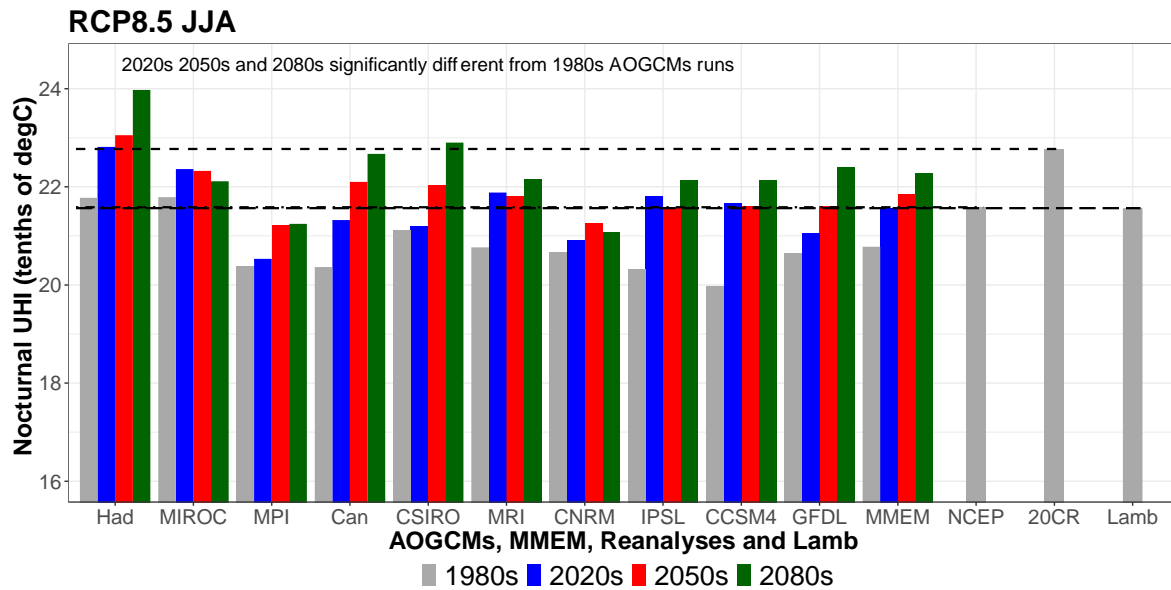
488

489

490

Figure 6. F-Score for LWTs associated with concurrent fluvial flooding-wind hazards during winter DJF. The F-Score is shown for each CMIP5 AOGCM, MMEM, NCEP, 20CR and Lamb's subjective catalogue for the 1980s, 2020s, 2050s and 2080s periods. The LWTs used for calculating the F-Score are associated with concurrent multi-basin fluvial flooding and wind hazards within Great Britain (GB) [25]. The 1980s MME F-Score were estimated from the mean of n=1,000 boot-strapped samples and all the future 2020s, 2050s and 2080s periods are significantly different from these, as the F-Score of the latter fall outside the 95% confidence intervals of the 1980s means. The AOGCMs 1980s confidence intervals bars are not shown for simplicity because they are vanishingly narrow. Dashed lines represent the reanalyses and Lamb's catalogue values.

Summer nocturnal UHI temperatures in tenths of °C for London (UK), were estimated for RCP8.5, by using UHI values obtained in a previous study [38] (Figure 7 and Section 2.4). Our results show that AOGCMs replicate nocturnal UHI temperatures, although there is a tendency for underestimation by the majority of AOGCMs except HadGEM2-ES and MIROC5 which show good agreement when compared to 20CR, NCEP and Lamb's subjective catalogue as per the F-Score (Figure 6). We also note that there is less variability within the MME than displayed in Figures 4 and 6. Lastly, almost all the AOGCMs and MMEM show a statistically significant increase in UHI by the end of 2100, that could translate into an increased multi-hazard risk from heatwave and poor air quality events associated with persistent A weather types [38,55,88,89]. The projected increase in the MMEM UHI between the 1980s and 2080s is 0.15 °C under RCP8.5. The AOGCMs that show the largest increase in nocturnal UHI temperatures between 1980s and 2080s are CanESM2, HadGEM2-ES and CCSM4 with respectively 0.23, 0.22 and 0.22 °C. Results for RCP4.5 agree with the RCP8.5 projections although the changes are less marked (Figure S5). Implied increases in the risk of urban air pollution hazards are potentially conservative given policies to phase out conventional cars in the UK by 2050.



491

492

Figure 7. As per Figure 6 but for London's nocturnal UHI in tenths of °C during summer JJA.

493

494

495

4. Discussion and Conclusions

496

497

498

499

500

501

502

503

504

505

506

507

508

509

510

511

512

513

514

515

516

517

518

519

520

As found in our analysis, greater A-type persistence and frequency during summer likely implies more blocking episodes with increased risk of poor air quality, drought and heatwaves [1,5,90,91]. A growing number of studies propose physical mechanisms that link Arctic Amplification (AA) [92] to more persistent weather patterns, which in turn enhance the likelihood of extreme weather events in the northern hemisphere mid-latitudes. The AA may affect the polar jet stream by making Rossby waves more meridional (or wavier) and by weakening its flow. A wavier and weaker jet stream in summer favours more persistent extreme weather and it is also thought to extend ridges northward, enhancing such effects [1–3,90,91,93–95]. In contrast, another study suggests that increasing trends in meridional extent of the jet stream, along with blocking events, may be an artefact of the methodologies used [85].

Our results support earlier analysis [54], and are consistent with the proposed mechanisms linking *observed* AA with mid-latitude weather extremes. On the one hand, AA could have limited effect on simulated CMIP5 blocking over Eurasia under RCP8.5 in the second half of the 21st century [97]. Other work, that makes use of three different algorithms for computing blocking (i.e. anomaly, absolute and hybrid methods) also shows an overall decrease in CMIP5 blocking events over the BI in winter DJF and summer JJA, during 2061-2090 (RCP8.5) [70]. Our findings for anticyclonic weather appear to contradict this. Although A-type persistence and frequency are equivalent to blocking *per se*, we would expect the studies to agree as both mechanisms involve high pressure weather systems. A common denominator between our findings and studies of blocking [70,97] is the underestimation of A-type/blocking events by CMIP5 models. However, further research is needed to reconcile apparently contradictory findings. Possible explanations are that results depend on the exact spatial domain and/or suite of AOGCMs analysed in each MME, as well as on the methodology used to define A-type days and blocking events.

521 In our study, less persistent C-types in autumn suggests lower likelihood of heavy rainfall, with
522 reduced recharge of soil moisture and aquifers at the start of the hydrological year, thereby favouring
523 winter droughts. Fewer cyclonic days may also translate into less frequent severe gales and fluvial
524 flooding episodes [49], as in GB extreme multi-basin fluvial flooding events are strongly associated
525 with C-type weather over time windows from 1 to 19 days [25]. Conversely, more frequent zonal
526 airflow (W-type) in winter may counteract some loss of precipitation from the C-type, especially
527 across higher elevation regions of the north and west BI where there is strong orographic
528 enhancement [98]. Such changes may also be attributed to AA, however, the physical mechanisms
529 linking AA to changes in northern hemisphere mid-latitude circulation currently remains an open
530 question.

531
532 From our analyses it is also possible to infer future changes with respect to multi-hazards [15,17],
533 through the F-Score and nocturnal UHI temperatures. Recent analyses show that in GB nearly
534 concurrent multi-basin fluvial flooding and extreme wind events are driven by selected LWTs mainly
535 associated with C- and W-types [25]. These multi-hazard events can generate significant economic
536 losses hence projections of such events may help in evaluating future risks and in improving
537 resilience. We show that during winter DJF our ensemble of AOGCMs overestimate the F-Score when
538 compared to 20CR, NCEP reanalyses and Lamb's subjective dataset. Even so, by the end of 2100 the
539 MMEM shows a statistically significant increase in the F-Score compared with the 1980s within those
540 same models, suggesting that the risk of concurrent fluvial flooding-wind impacts may become more
541 severe in a warmer world. The two AOGCMs that show the closest agreement with the reanalyses
542 are HadGEM2-ES and MIROC5.

543
544 Our results for nocturnal UHI temperatures in London modelled by AOGCMs agree with 20CR,
545 NCEP and Lamb's subjective datasets, although they are slightly underestimated for the 1980s. As
546 per the F-Score, HadGEM2-ES and MIROC5 are the AOGCMs that best represent the reanalyses and,
547 therefore, they may be preferred when assessing these two multi-hazard scenarios. Nocturnal UHI
548 severity could increase by 2100 under RCP8.5 (MMEM). Our results confirm an increasing trend of
549 ~0.3 °C in nocturnal UHI in London found in an earlier study over the observational period 1950-
550 2006 [38]. Our findings are also in line with the UK Climate Projections Science Report 2009 [99] which
551 suggests that intense UHI events are highly correlated with A-type weather patterns, and that in
552 London, intense UHI summer events could become more severe in the future [50]. However, further
553 analysis of projections of UHI is needed with a larger AOGCM ensemble to better account for
554 uncertainty. Our results for UHI also assume an unchanging urban landscape and pattern of artificial
555 heat sources. Nevertheless, the present findings, when viewed as a significant increase in persistence
556 and frequency of A-type weather pattern, suggest more favourable conditions for heatwaves and
557 poor air quality events in London that could negatively impact human health [38,50,55,88,89].

558
559 Finally, we have illustrated how changes in the persistence and frequency of weather patterns
560 are useful diagnostics of climate model realism and can translate into regional to local weather and
561 climate risks scenarios, which could be helpful for developing narratives for decision-makers.
562 However, caution needs to be taken when qualitatively converting synoptic weather pattern changes
563 into local variability because AOGCM skill in reproducing climatic variables at local scales varies

564 significantly and is not always consistent with observations. This is particularly true for precipitation
565 where, for example, pressure fields alone are not able to provide reliable local projections [43]. In our
566 work, the two reanalyses products and Lamb's subjective catalogue show different results. Thus, it is
567 difficult at this stage to suggest a preferred observational dataset for AOGCM validation. However,
568 the objective classifications have the advantage of consistency over the subjective Lamb's catalogue.
569 Our suggestion, therefore, would be to use a large ensemble of open source reanalyses products, to
570 better account for uncertainty coming from products with different characteristics.

571

572 With the UK Climate Projections 2018 now partly released and work underway for the third UK
573 Climate Change Risk Assessment, weather pattern analysis could help to both evaluate the new
574 projections and offer ways of explaining changes that are intelligible to a range of user communities.
575 Similar links to persistence could be made in other regions with established weather pattern
576 typologies, such as the *Grosswetterlagen* for Europe [100], hydrologically important weather types in
577 the contiguous United States [101] and Spatial Synoptic Classification for North America [102].

578

579

580 **Supplementary Materials:** *Supplementary datasets. Supplementary Data and Methods. Supplementary Figures*, Figure
581 S1: As per Figure 3 but for RCP4.5, Figure S2: As per Figure 4 but for RCP4.5, Figure S3: As per Figure 5 but for
582 RCP4.5, Figure S4: As per Figure 6 but for RCP4.5, Figure S5: As per Figure 7 but for RCP4.5. *Supplementary*
583 *Tables*, Table S1: MME statistical significance of LWTs persistence for RCP8.5, Table S2: The same as Table S1 but
584 for RCP4.5, Table S3: Sen’s slopes of MMEM seasonal LWTs frequencies for RCP8.5 and RCP4.5.

585
586 **Author Contributions:** Conceptualization, PDL and RW; methodology, PDL, RW and CF; software, CH and
587 PDL; formal analysis, PDL; data curation, PDL and CH; writing—original draft preparation, PDL; writing—
588 review and editing, PDL, RW, JH, CF and GL; supervision, RW, JH and GL.

589
590 **Funding:** PDL was funded by a Natural Environment Research Council studentship awarded through the
591 Central England NERC Training Alliance (CENTA <http://www.centa.org.uk/>; Grant No. NE/L002493/1) and by
592 Loughborough University. CF was supported by the Collaborative Research Centre TRR 181 “Energy Transfer
593 in Atmosphere and Ocean”, funded by the Deutsche Forschungsgemeinschaft (DFG, German Research
594 Foundation <https://www.dfg.de/en/>) – Projektnummer 274762653. The APC was funded by CENTA NERC.

595
596 **Conflicts of Interest:** The authors declare no conflict of interest. The funders had no role in the design of the
597 study; in the collection, analyses, or interpretation of data; in the writing of the manuscript, or in the decision to
598 publish the results.

599

600

601

602

603

604

605

606

607

608

609

610

611

612

613

614

615

616

617 **References**

- 618 1. Coumou D, Di Capua G, Vavrus S, Wang L, Wang S. The influence of Arctic amplification
619 on mid-latitude summer circulation. *Nat Commun* 2018;9:2959. doi:10.1038/s41467-018-
620 05256-8.
- 621 2. Francis J, Skific N. Evidence linking rapid Arctic warming to mid-latitude weather patterns.
622 *Philos Trans R Soc London A Math Phys Eng Sci* 2015;373. doi:10.1098/rsta.2014.0170.
- 623 3. Francis JA, Vavrus SJ. Evidence linking Arctic amplification to extreme weather in mid-
624 latitudes. *Geophys Res Lett* 2012;39. doi:10.1029/2012GL051000.
- 625 4. Francis JA, Vavrus SJ. Evidence for a wavier jet stream in response to rapid Arctic warming.
626 *Environ Res Lett* 2015;10:14005.
- 627 5. Munich Re. Natural catastrophes 2014: Analyses, assessments, positions. 2015.
- 628 6. Munich Re. NatCatSERVICE - Natural catastrophes in 2018. 2019.
- 629 7. Stott PA, Stone DA, Allen MR. Human contribution to the European heatwave of 2003.
630 *Nature* 2004;432:610–4. doi:10.1038/nature03089.
- 631 8. Barriopedro D, Fischer EM, Luterbacher J, Trigo RM, García-Herrera R. The Hot Summer of
632 2010: Redrawing the Temperature Record Map of Europe. *Science* (80-) 2011;332:220 LP –
633 224. doi:10.1126/science.1201224.
- 634 9. Bastos A, Gouveia CM, Trigo RM, Running SW. Analysing the spatio-temporal impacts of
635 the 2003 and 2010 extreme heatwaves on plant productivity in Europe. *Biogeosciences*
636 2014;11:3421–35. doi:10.5194/bg-11-3421-2014.
- 637 10. Le Tertre A, Lefranc A, Eilstein D, Declercq C, Medina S, Blanchard M, et al. Impact of the
638 2003 Heatwave on All-Cause Mortality in 9 French Cities. *Epidemiology* 2006;17:75–9.
- 639 11. Sun Y, Zhang X, Zwiers FW, Song L, Wan H, Hu T, et al. Rapid increase in the risk of
640 extreme summer heat in Eastern China. *Nat Clim Chang* 2014;4:1082.
- 641 12. Muchan K, Lewis M, Hannaford J, Parry S. The winter storms of 2013/2014 in the UK:
642 hydrological responses and impacts. *Weather* 2015;70:55–61. doi:10.1002/wea.2469.
- 643 13. Kendon M, McCarthy M. The UK's wet and stormy winter of 2013/2014. *Weather*
644 2015;70:40–7. doi:10.1002/wea.2465.
- 645 14. Matthews T, Murphy C, Wilby RL, Harrigan S. Stormiest winter on record for Ireland and
646 UK. *Nat Publ Gr* 2014;4:738–40. doi:10.1038/nclimate2336.
- 647 15. Zscheischler J, Westra S, van den Hurk BJJM, Seneviratne SI, Ward PJ, Pitman A, et al.
648 Future climate risk from compound events. *Nat Clim Chang* 2018;8:469–77.
649 doi:10.1038/s41558-018-0156-3.

- 650 16. AghaKouchak A, Huning LS, Mazdiyasn O, Mallakpour I, Chiang F, Sadegh M, et al. How
651 do natural hazards cascade to cause disasters? *Nature* 2018;561:458–60. doi:10.1038/d41586-
652 018-06783-6.
- 653 17. Gill JC, Malamud BD. Reviewing and visualizing the interactions of natural hazards. *Rev*
654 *Geophys* 2014;52:680–722. doi:10.1002/2013RG000445.
- 655 18. Kappes MS, Keiler M, von Elverfeldt K, Glade T. Challenges of analyzing multi-hazard risk:
656 a review. *Nat Hazards* 2012;64:1925–58. doi:10.1007/s11069-012-0294-2.
- 657 19. Terzi S, Torresan S, Schneiderbauer S, Critto A, Zebisch M, Marcomini A. Multi-risk
658 assessment in mountain regions: A review of modelling approaches for climate change
659 adaptation. *J Environ Manage* 2019;232:759–71.
660 doi:https://doi.org/10.1016/j.jenvman.2018.11.100.
- 661 20. Forzieri G, Feyen L, Russo S, Voudoukas M, Alfieri L, Outten S, et al. Multi-hazard
662 assessment in Europe under climate change. *Clim Change* 2016;137:105–19.
663 doi:10.1007/s10584-016-1661-x.
- 664 21. Gallina V, Torresan S, Critto A, Sperotto A, Glade T, Marcomini A. A review of multi-risk
665 methodologies for natural hazards: Consequences and challenges for a climate change
666 impact assessment. *J Environ Manage* 2016;168:123–32.
- 667 22. UNDRR. Sendai Framework for Disaster Risk Reduction 2015–2030. 2015.
- 668 23. Leonard M, Westra S, Phatak A, Lambert M, van den Hurk B, McInnes K, et al. A compound
669 event framework for understanding extreme impacts. *Wiley Interdiscip Rev Clim Chang*
670 2014;5:113–28. doi:10.1002/wcc.252.
- 671 24. Kargel JS, Leonard GJ, Shugar DH, Haritashya UK, Bevington A, Fielding EJ, et al.
672 Geomorphic and geologic controls of geohazards induced by Nepal’s 2015 Gorkha
673 earthquake. *Science* (80-) 2016;351.
- 674 25. De Luca P, Hillier JK, Wilby RL, Quinn NW, Harrigan S. Extreme multi-basin flooding
675 linked with extra-tropical cyclones. *Environ Res Lett* 2017;12:114009. doi:10.1088/1748-
676 9326/aa868e.
- 677 26. Ward PJ, Couasnon A, Eilander D, Haigh ID, Hendry A, Muis S, et al. Dependence between
678 high sea-level and high river discharge increases flood hazard in global deltas and estuaries.
679 *Environ Res Lett* 2018;13:84012. doi:10.1088/1748-9326/aad400.
- 680 27. Bevacqua E, Maraun D, Voudoukas MI, Voukouvalas E, Vrac M, Mentaschi L, et al. Higher
681 probability of compound flooding from precipitation and storm surge in Europe under
682 anthropogenic climate change. *Sci Adv* 2019;5:eaaw5531. doi:10.1126/sciadv.aaw5531.
- 683 28. Khanal S, Ridder N, de Vries H, Terink W, van den Hurk B. Storm Surge and Extreme River
684 Discharge: A Compound Event Analysis Using Ensemble Impact Modeling . *Front Earth*

- 685 Sci 2019;7:224.
- 686 29. Collet L, Harrigan S, Prudhomme C, Formetta G, Beevers L. Future hot-spots for hydro-
687 hazards in Great Britain: a probabilistic assessment. *Hydrol Earth Syst Sci* 2018;22:5387–401.
688 doi:10.5194/hess-22-5387-2018.
- 689 30. De Luca P, Messori G, Wilby RL, Mazzoleni M, Di Baldassarre G. Concurrent wet and dry
690 hydrological extremes at the global scale. *Earth Syst Dynam Discuss* 2019:1–24.
691 doi:10.5194/esd-2019-27.
- 692 31. Visser-Quinn A, Beevers L, Collet L, Formetta G, Smith K, Wanders N, et al. Spatio-temporal
693 analysis of compound hydro-hazard extremes across the UK. *Adv Water Resour*
694 2019;130:77–90. doi:https://doi.org/10.1016/j.advwatres.2019.05.019.
- 695 32. De Luca P, Messori G, Faranda D. Dynamical Systems Theory Sheds New Light on
696 Compound Climate Extremes in Europe and Eastern North America. *EarthArXiv* 2019.
697 doi:https://doi.org/10.31223/osf.io/qdn5w.
- 698 33. Lamb HH. British Isles Weather types and a register of daily sequence of circulation
699 patterns, 1861-1971. *Geophysical Memoir* 116, London, HMSO; 1972.
- 700 34. Jenkinson AF, Collison FP. An Initial Climatology of Gales over the North Sea. *Synoptic*
701 *Climatology Branch Memorandum No. 62*, Meteorological Office, Bracknell; 1977.
- 702 35. Jones PD, Hulme M, Briffa KR. A comparison of Lamb circulation types with an objective
703 classification scheme. *Int J Climatol* 1993;13:655–63. doi:10.1002/joc.3370130606.
- 704 36. Jones PD, Harpham C, Briffa KR. Lamb weather types derived from reanalysis products. *Int*
705 *J Climatol* 2013;33:1129–39. doi:10.1002/joc.3498.
- 706 37. Jones PD, Osborn TJ, Harpham C, Briffa KR. The development of Lamb weather types: From
707 subjective analysis of weather charts to objective approaches using reanalyses. *Weather*
708 2014;69:128–32. doi:10.1002/wea.2255.
- 709 38. Wilby RL, Jones PD, Lister DH. Decadal variations in the nocturnal heat island of London.
710 *Weather* 2011;66:59–64. doi:10.1002/wea.679.
- 711 39. Merz B, Aerts J, Arnbjerg-Nielsen K, Baldi M, Becker A, Bichet A, et al. Floods and climate:
712 emerging perspectives for flood risk assessment and management. *Nat Hazards Earth Syst*
713 *Sci* 2014;14:1921–42. doi:10.5194/nhess-14-1921-2014.
- 714 40. Conticello F, Cioffi F, Merz B, Lall U. An event synchronization method to link heavy
715 rainfall events and large-scale atmospheric circulation features. *Int J Climatol* 2018;38:1421–
716 37. doi:10.1002/joc.5255.
- 717 41. Farnham DJ, Doss-Gollin J, Lall U. Regional Extreme Precipitation Events: Robust Inference
718 From Credibly Simulated GCM Variables. *Water Resour Res* 2018;54:3809–24.

- 719 doi:10.1002/2017WR021318.
- 720 42. Murawski A, Vorogushyn S, Bürger G, Gerlitz L, Merz B. Do Changing Weather Types
721 Explain Observed Climatic Trends in the Rhine Basin? An Analysis of Within- and Between-
722 Type Changes. *J Geophys Res Atmos* 2018;123:1562–84. doi:10.1002/2017JD026654.
- 723 43. Murawski A, Bürger G, Vorogushyn S, Merz B. Can local climate variability be explained by
724 weather patterns? A multi-station evaluation for the Rhine basin. *Hydrol Earth Syst Sci*
725 2016;20:4283–306. doi:10.5194/hess-20-4283-2016.
- 726 44. Pattison I, Lane SN. The relationship between Lamb weather types and long-term changes in
727 flood frequency, River Eden, UK. *Int J Climatol* 2012;32:1971–89. doi:10.1002/joc.2415.
- 728 45. Matthews T, Murphy C, Wilby RL, Harrigan S. A cyclone climatology of the British-Irish
729 Isles 1871–2012. *Int J Climatol* 2016;36:1299–312. doi:10.1002/joc.4425.
- 730 46. Ridder N, de Vries H, Drijfhout S. The role of atmospheric rivers in compound events
731 consisting of heavy precipitation and high storm surges along the Dutch coast. *Nat Hazards*
732 *Earth Syst Sci* 2018;18:3311–26. doi:10.5194/nhess-18-3311-2018.
- 733 47. Wilby RL, Wigley TML. Downscaling general circulation model output: a review of methods
734 and limitations. *Prog Phys Geogr Earth Environ* 1997;21:530–48.
735 doi:10.1177/030913339702100403.
- 736 48. Xu H, Corte-Real J, Qian B. Developing daily precipitation scenarios for climate change
737 impact studies in the Guadiana and the Tejo basins. *Hydrol Earth Syst Sci* 2007;11:1161–73.
738 doi:10.5194/hess-11-1161-2007.
- 739 49. Wilby RL, Quinn NW. Reconstructing multi-decadal variations in fluvial flood risk using
740 atmospheric circulation patterns. *J Hydrol* 2013;487:109–21. doi:10.1016/j.jhydrol.2013.02.038.
- 741 50. Wilby RL. Constructing Climate Change Scenarios of Urban Heat Island Intensity and Air
742 Quality. *Environ Plan B Plan Des* 2008;35:902–19. doi:10.1068/b33066t.
- 743 51. Burt TP, Jones PD, Howden NJK. An analysis of rainfall across the British Isles in the 1870s.
744 *Int J Climatol* 2015;35:2934–47. doi:10.1002/joc.4184.
- 745 52. Tyler JJ, Jones M, Arrowsmith C, Allott T, Leng MJ. Spatial patterns in the oxygen isotope
746 composition of daily rainfall in the British Isles. *Clim Dyn* 2016;47:1971–87.
747 doi:10.1007/s00382-015-2945-y.
- 748 53. Stryhal J, Huth R. Trends in winter circulation over the British Isles and central Europe in
749 twenty-first century projections by 25 CMIP5 GCMs. *Clim Dyn* 2018;0:0. doi:10.1007/s00382-
750 018-4178-3.
- 751 54. Otero N, Sillmann J, Butler T. Assessment of an extended version of the Jenkinson–Collison
752 classification on CMIP5 models over Europe. *Clim Dyn* 2018;50:1559–79. doi:10.1007/s00382-

- 753 017-3705-y.
- 754 55. Pope RJ, Butt EW, Chipperfield MP, Doherty RM, Fenech S, Schmidt A, et al. The impact of
755 synoptic weather on UK surface ozone and implications for premature mortality. *Environ*
756 *Res Lett* 2016;11. doi:10.1088/1748-9326/11/12/124004.
- 757 56. Burt TP, Ferranti EJS. Changing patterns of heavy rainfall in upland areas: a case study from
758 northern England. *Int J Climatol* 2012;32:518–32. doi:10.1002/joc.2287.
- 759 57. Jones PD, Harpham C, Lister D. Long-term trends in gale days and storminess for the
760 Falkland Islands. *Int J Climatol* 2016;36:1413–27. doi:10.1002/joc.4434.
- 761 58. Wetterhall F, Pappenberger F, He Y, Freer J, Cloke HL. Conditioning model output statistics
762 of regional climate model precipitation on circulation patterns. *Nonlinear Process Geophys*
763 2012;19:623–33. doi:10.5194/npg-19-623-2012.
- 764 59. Richardson D, Fowler HJ, Kilsby CG, Neal R. A new precipitation and drought climatology
765 based on weather patterns. *Int J Climatol* 2018;38:630–48. doi:10.1002/joc.5199.
- 766 60. Wilby RL, Dalgleish HY, Foster IDL. The impact of weather patterns on historic and
767 contemporary catchment sediment yields. *Earth Surf Process Landforms* 1997;22:353–63.
- 768 61. Blenkinsop S, Chan SC, Kendon EJ, Roberts NM, Fowler HJ. Temperature influences on
769 intense UK hourly precipitation and dependency on large-scale circulation. *Environ Res Lett*
770 2015;10:54021. doi:10.1088/1748-9326/10/5/054021.
- 771 62. Fowler HJ, Kilsby CG. A weather-type approach to analysing water resource drought in the
772 Yorkshire region from 1881 to 1998. *J Hydrol* 2002;262:177–92.
773 doi:[https://doi.org/10.1016/S0022-1694\(02\)00034-3](https://doi.org/10.1016/S0022-1694(02)00034-3).
- 774 63. Wilby RL. The influence of variable weather patterns on river water quantity and quality
775 regimes. *Int J Climatol* 1993;13:447–59. doi:10.1002/joc.3370130408.
- 776 64. Tang L, Chen D, Karlsson P, Gu Y, Ou T. Synoptic circulation and its influence on spring
777 and summer surface ozone concentrations in southern Sweden. *Boreal Environ Res*
778 2009;14:889–902.
- 779 65. Grundström M, Hak C, Chen D, Hallquist M, Pleijel H. Variation and co-variation of PM10,
780 particle number concentration, NOx and NO2 in the urban air – Relationships with wind
781 speed, vertical temperature gradient and weather type. *Atmos Environ* 2015;120:317–27.
782 doi:<https://doi.org/10.1016/j.atmosenv.2015.08.057>.
- 783 66. Cortesi N, Gonzalez-Hidalgo JC, Trigo RM, Ramos AM. Weather types and spatial
784 variability of precipitation in the Iberian Peninsula. *Int J Climatol* 2014;34:2661–77.
785 doi:10.1002/joc.3866.
- 786 67. Domínguez-Castro F, Ramos AM, García-Herrera R, Trigo RM. Iberian extreme precipitation

- 787 1855/1856: an analysis from early instrumental observations and documentary sources. *Int J*
788 *Climatol* 2015;35:142–53. doi:10.1002/joc.3973.
- 789 68. Eiras-Barca J, Lorenzo N, Taboada J, Robles A, Miguez-Macho G. On the relationship
790 between atmospheric rivers, weather types and floods in Galicia (NW Spain). *Nat Hazards*
791 *Earth Syst Sci* 2018;18:1633–45. doi:10.5194/nhess-18-1633-2018.
- 792 69. Lorenzo MN, Taboada JJ, Gimeno L. Links between circulation weather types and
793 teleconnection patterns and their influence on precipitation patterns in Galicia (NW Spain).
794 *Int J Climatol* 2008;28:1493–505. doi:10.1002/joc.1646.
- 795 70. Woollings T, Barriopedro D, Methven J, Son S-W, Martius O, Harvey B, et al. Blocking and
796 its Response to Climate Change. *Curr Clim Chang Reports* 2018. doi:10.1007/s40641-018-
797 0108-z.
- 798 71. Taylor KE, Stouffer RJ, Meehl GA. An Overview of CMIP5 and the Experiment Design. *Bull*
799 *Am Meteorol Soc* 2011;93:485–98. doi:10.1175/BAMS-D-11-00094.1.
- 800 72. Compo GP, Whitaker JS, Sardeshmukh PD, Matsui N, Allan RJ, Yin X, et al. The Twentieth
801 Century Reanalysis Project. *Q J R Meteorol Soc* 2011;137:1–28. doi:10.1002/qj.776.
- 802 73. Kalnay E, Kanamitsu M, Kistler R, Collins W, Deaven D, Gandin L, et al. The NCEP/NCAR
803 40-Year Reanalysis Project. *Bull Am Meteorol Soc* 1996;77:437–71.
804 doi:https://doi.org/10.1175/1520-0477(1996)077<0437:TNYRP>2.0.CO;2.
- 805 74. Hulme M, Barrow E. *Climate of the British Isles: present, past and future*. London:
806 Routledge; 1997.
- 807 75. Jones PD, Kelly PM. Principal component analysis of the Lamb Catalogue of Daily Weather
808 Types: Part 1, annual frequencies. *Int J Climatol* 1982;2:147–57.
- 809 76. Lamb HH. Types and spells of weather around the year in the British Isles : Annual trends,
810 seasonal structure of the year, singularities. *Q J R Meteorol Soc* 1950;76:393–429.
811 doi:10.1002/qj.49707633005.
- 812 77. Hulme M, Briffa KR, Jones PD, Senior CA, Briffal KR, Jones PD, et al. Validation of GCM
813 control simulations using indices of daily airflow types over the British Isles. *Clim Dyn*
814 1993;9:95–105. doi:10.1007/BF00210012.
- 815 78. Diaz-Nieto J, Wilby RL. A comparison of statistical downscaling and climate change factor
816 methods: impacts on low flows in the River Thames, United Kingdom. *Clim Change*
817 2005;69:245–68. doi:https://doi.org/10.1007/s10584-005-1157-6.
- 818 79. Li T, Horton RM, Kinney PL. Projections of seasonal patterns in temperature- related deaths
819 for Manhattan, New York. *Nat Clim Chang* 2013;3:717.
- 820 80. Dolinar EK, Dong X, Xi B. Evaluation and intercomparison of clouds, precipitation, and

- 821 radiation budgets in recent reanalyses using satellite-surface observations. *Clim Dyn*
822 2016;46:2123–44. doi:10.1007/s00382-015-2693-z.
- 823 81. Decker M, Brunke MA, Wang Z, Sakaguchi K, Zeng X, Bosilovich MG. Evaluation of the
824 Reanalysis Products from GSFC, NCEP, and ECMWF Using Flux Tower Observations. *J*
825 *Clim* 2011;25:1916–44. doi:10.1175/JCLI-D-11-00004.1.
- 826 82. Wilby RL. Stochastic weather type simulation for regional climate change impact
827 assessment. *Water Resour Res* 1994;30:3395–403. doi:10.1029/94WR01840.
- 828 83. Gagniuc PA. *Markov Chains: From Theory to Implementation and Experimentation*. USA,
829 NJ: John Wiley & Sons; 2017. doi:10.1002/9781119387596.
- 830 84. Spedicato GA. Discrete Time Markov Chains with R. *R J* 2017;9:84–104.
- 831 85. Mann HB, Whitney DR. On a Test of Whether one of Two Random Variables is
832 Stochastically Larger than the Other. *Ann Math Stat* 1947;18:50–60.
833 doi:10.1214/aoms/1177730491.
- 834 86. Hamed KH, Ramachandra Rao A. A modified Mann-Kendall trend test for autocorrelated
835 data. *J Hydrol* 1998;204:182–96. doi:https://doi.org/10.1016/S0022-1694(97)00125-X.
- 836 87. Sen PK. Estimates of the Regression Coefficient Based on Kendall's Tau. *J Am Stat Assoc*
837 1968;63:1379–89. doi:10.1080/01621459.1968.10480934.
- 838 88. O'Hare GPP, Wilby RL. A Review of Ozone Pollution in the United Kingdom and Ireland
839 with an Analysis Using Lamb Weather Types. *Geogr J* 1995;161:1–20. doi:10.2307/3059923.
- 840 89. Pope RJ, Savage NH, Chipperfield MP, Arnold SR, Osborn TJ. The influence of synoptic
841 weather regimes on UK air quality: analysis of satellite column NO₂. *Atmos Sci Lett*
842 2014;15:211–7. doi:10.1002/asl2.492.
- 843 90. Tang Q, Zhang X, Francis JA. Extreme summer weather in northern mid-latitudes linked to a
844 vanishing cryosphere. *Nat Clim Chang* 2013;4:45.
- 845 91. Pfliegerer P, Schleussner C-F, Kornhuber K, Coumou D. Summer weather becomes more
846 persistent in a 2 °C world. *Nat Clim Chang* 2019. doi:10.1038/s41558-019-0555-0.
- 847 92. Screen JA, Simmonds I. The central role of diminishing sea ice in recent Arctic temperature
848 amplification. *Nature* 2010;464:1334.
- 849 93. Cohen J, Screen JA, Furtado JC, Barlow M, Whittleston D, Coumou D, et al. Recent Arctic
850 amplification and extreme mid-latitude weather. *Nat Geosci* 2014;7:627.
- 851 94. Francis JA. Why Are Arctic Linkages to Extreme Weather Still up in the Air? *Bull Am*
852 *Meteorol Soc* 2017;98:2551–7. doi:10.1175/BAMS-D-17-0006.1.

- 853 95. Francis JA, Vavrus SJ, Cohen J. Amplified Arctic warming and mid-latitude weather: new
854 perspectives on emerging connections. *Wiley Interdiscip Rev Clim Chang* 2017;8:e474.
855 doi:10.1002/wcc.474.
- 856 96. Barnes EA. Revisiting the evidence linking Arctic amplification to extreme weather in
857 midlatitudes. *Geophys Res Lett* 2013;40:4734–9. doi:10.1002/grl.50880.
- 858 97. Woollings T, Harvey B, Masato G. Arctic warming, atmospheric blocking and cold European
859 winters in CMIP5 models. *Environ Res Lett* 2014;9:14002.
- 860 98. Burt TP, Howden NJK. North Atlantic Oscillation amplifies orographic precipitation and
861 river flow in upland Britain. *Water Resour Res* 2013;49:3504–15. doi:10.1002/wrcr.20297.
- 862 99. Murphy JM, Sexton DMH, Jenkins GJ, Boorman PM, Booth BBB, Brown CC, et al. UK
863 Climate Projections Science Report: Climate change projections. Exeter: 2009.
- 864 100. Hess P, Brezowsky H. Katalog der Großwetterlagen Europas. Berichte des Deutschen
865 Wetterdienstes in der US-Zone 33. Deutscher Wetterdienst in d. US-Zone: Bad Kissingen.;
866 1952.
- 867 101. Prein AF, Bukovsky MS, Mearns LO, Bruyère CL, Done JM. Simulating North American
868 Weather Types With Regional Climate Models. *Front Environ Sci* 2019;7:36.
- 869 102. Kalkstein LS, Nichols MC, Barthel CD, Greene JS. A new spatial synoptic classification:
870 application to air-mass analysis. *Int J Climatol* 1996;16:983–1004. doi:10.1002/(SICI)1097-
871 0088(199609)16:9<983::AID-JOC61>3.0.CO;2-N.
- 872